Applied Surface Science 356 (2015) 978–985

Contents lists available at ScienceDirect

Applied Surface Science

journal homepage: www.elsevier.com/locate/apsusc

# Study on the growth mechanism and optical properties of sputtered lead selenide thin films

Xigui Sun [a], Kewei Gao [a], Xiaolu Pang [a,*], Huisheng Yang [a], Alex A. Volinsky [b]

[a] Department of Materials Physics and Chemistry, University of Science and Technology Beijing, Beijing 100083, China
[b] Department of Mechanical Engineering, University of South Florida, Tampa, FL 33620, USA

ARTICLE INFO

*Article history:*
Received 13 May 2015
Received in revised form 21 August 2015
Accepted 24 August 2015

*Keywords:*
Lead selenide
Magnetron sputtering
Deposition temperature
Growth mechanism
Optical properties

ABSTRACT

Lead selenide thin films with different microstructure were deposited on Si (100) substrates using magnetron sputtering at 50 °C, 150 °C and 250 °C, respectively. The crystal structure of the sputtered PbSe thin films varies from amorphous crystalline to columnar grain, and then to double-layer (nanocrystalline layer and columnar grain layer) structure as the deposition temperature increases, which is due to the dominating growth mode of the thin films changes from Frank–van der Merwe (or layer-by-layer) growth mode at 50 °C to Volmer–Weber (or 3D island) growth mode at 150 °C, and then to Stranski–Krastanow (or 3D island-on-wetting-layer) growth mode at 250 °C. The growth mechanism of the sputtered PbSe thin films is mainly dominated by the surface and strain energy contributions. Moreover, the strain energy contribution is more prominent when the deposition temperature is less than 180 °C, while, the surface energy contribution is more prominent when the deposition temperature is higher than 180 °C. The absorption spectra of the sputtered PbSe thin films are in 3.1–5 μm range. Besides, the sputtered PbSe thin film prepared at 250 °C has two different optical band gaps due to its unique double-layer structure. According to the theoretical calculation results, the variation of the band gap with the deposition temperature is determined by the shift of the valence band maximum with the lattice constant.



## 1. Introduction

Lead chalcogenides are typical narrow band gap materials with the absorption range of 3–30 μm corresponding to the medium and far infrared range [1], which leads to wide application as infrared detectors [2–4], solar cells [5,6] and laser diodes [7–9]. In recent years, lead selenide (PbSe) thin films have aroused great concern due to high photoelectric sensitivity and stability even at room temperature compared with other lead chalcogenides, such as PbS, PbTe, etc. [10–14]. Generally, the band gap of the pure bulk PbSe materials is about 0.27 eV at room temperature, however, it can be modified by varying the composition and microstructure, which leads to the application of the tunable mid-infrared lasers [15]. Besides, the PbSe material has relatively large Bohr radius (46 nm at 300 K), leading to the remarkable quantum confinement effect even in the large crystals [16].

Generally, the composition and microstructure of the PbSe thin films can be varied by changing the preparation methods and corresponding parameters. Until now, the PbSe thin films have been successfully prepared by many chemical, electrochemical and physical methods, such as chemical bath deposition [17], electrochemical deposition [10], thermal evaporation [18], pulsed laser deposition [19] and molecular beam epitaxy [20], etc. In recent years, magnetron sputtering has been widely used to prepare semiconductor thin films due to its low cost, easy handling and high quality products compared with other preparation methods [21]. Besides, the sputtering parameters during the deposition process can be controlled precisely, which is important to obtain the PbSe thin films with specific properties [22]. And based on our previous researches, in magnetron sputtering it is much easier to modify the PbSe thin films structure, compared with other methods. However, to our knowledge, the growth of the PbSe thin films by magnetron sputtering has been rarely reported, and it is essential to study the potential of this method to prepare PbSe thin films.

There are mainly four parameters, deposition temperature, sputtering power, gas flux and deposition time, can be varied during the sputtering process, which can intensively affect the optical properties of the obtained PbSe thin films. On the other hand, the optical properties of the PbSe thin films are mainly determined by their microstructure. And among these four parameters, the deposition temperature is suggested to be the most important parameter which strongly influences the film structure over a

* Corresponding author. Tel.: +86 10 82376048; fax: +86 10 82376048.
*E-mail address:* pangxl@mater.ustb.edu.cn (X. Pang).

http://dx.doi.org/10.1016/j.apsusc.2015.08.195
0169-4332/

narrow temperature range. Shandalov et al. [23] have found that a transition from the nano-crystal growth mode to the columnar grain growth mode as the temperature increases when using the chemical bath deposition to deposit PbSe thin films, which is attributed to the transition from cluster growth mechanism in the initial stages of growth to ion-by-ion growth.

In the present work, the PbSe thin films were prepared using magnetron sputtering at three different deposition temperatures of 50 °C, 150 °C and 250 °C, respectively. The morphology, crystal structure and optical properties of the sputtered PbSe thin films were characterized by field emission scanning electron microscope (FE-SEM), X-ray diffraction (XRD), X-ray photoelectron spectroscopy (XPS) and Fourier transform infrared spectroscopy (FT-IR). The growth mechanism of the sputtered PbSe thin films at different deposition temperatures was studied in detail by using the theoretical calculation and experiments results. Besides, the effects of the microstructure on the optical properties were studied.

## 2. Experimental

The PbSe thin films were grown on Si (1 0 0) substrates by using the PM500-S magnetron sputtering system equipped with the MF-5K medium frequency sputtering power source under $5 \times 10^{-3}$ Pa base pressure. Three different deposition temperatures (50 °C, 150 °C and 250 °C) were chosen, and the obtained samples were labeled as PbSe-50, PbSe-150 and PbSe-250, respectively. During the sputtering process, other sputtering parameters remain unchanged: 150 W sputtering power, 60 min deposition time and 30 sccm argon gas flux. The PbSe alloy targets ($n_{Pb}$:$n_{Se}$ = 1:1) used in this research were hot pressed from the PbSe powders with 99.99% purity.

The cross-section morphology of the sputtered PbSe thin films was characterized by FE-SEM (Zeiss Auriga) with 15 kV operating voltage. The crystal structure of the thin films was studied using the anode diffractometer (Dmax-RB 12 KW, Rigaku) with the Cu $K\alpha$ radiation source, $\lambda$ = 1.5406 Å. In order to study the difference of the chemical states on and beneath the film surface, further XPS tests were performed using the AXIS ULTRA$^{DLD}$ (SHIMADZU) X-ray photoelectron spectrometer before and after the film surface was etched for 10 s by $Ar^+$ with 3000 eV etching energy. The infrared absorption spectra of the sputtered PbSe thin films were obtained by the Excalibur 3100 Fourier transform infrared spectrometer from 4000 $cm^{-1}$ to 400 $cm^{-1}$ with 2 $cm^{-1}$ resolution at room temperature.

## 3. Results and discussion

### 3.1. Microstructure

The cross-section morphology of the sputtered PbSe thin films varied from the equiaxed grains to columnar grains, and then to double-layer structure (nano-crystalline layer and columnar grain layer) with the deposition temperature, as shown in Fig. 1, which is attributed to the evolution of the growth mechanism of sputtered thin films discussed later.

The crystal structure of the sputtered PbSe thin films was studied by using XRD with the 2$\theta$ angle range of 10–65°, as shown in Fig. 2(a).

The crystal structure, especially the main diffraction peaks and the crystallinity of the sputtered PbSe thin films, varied with the deposition temperature. In addition, in all three samples no peaks belonging to other compounds are observed, which is attributed to their low content confirmed by the XPS results.

At low temperature (50 °C), an almost amorphous PbSe thin film was obtained due to the low migration activity of the Pb and Se atoms on the substrate surface, and consequently the crystal atoms distributed randomly with short range order [23,24]. The Frank–van der Merwe (or layer-by-layer) growth mode is supposed to dominate at this temperature, considering the difficulty of the

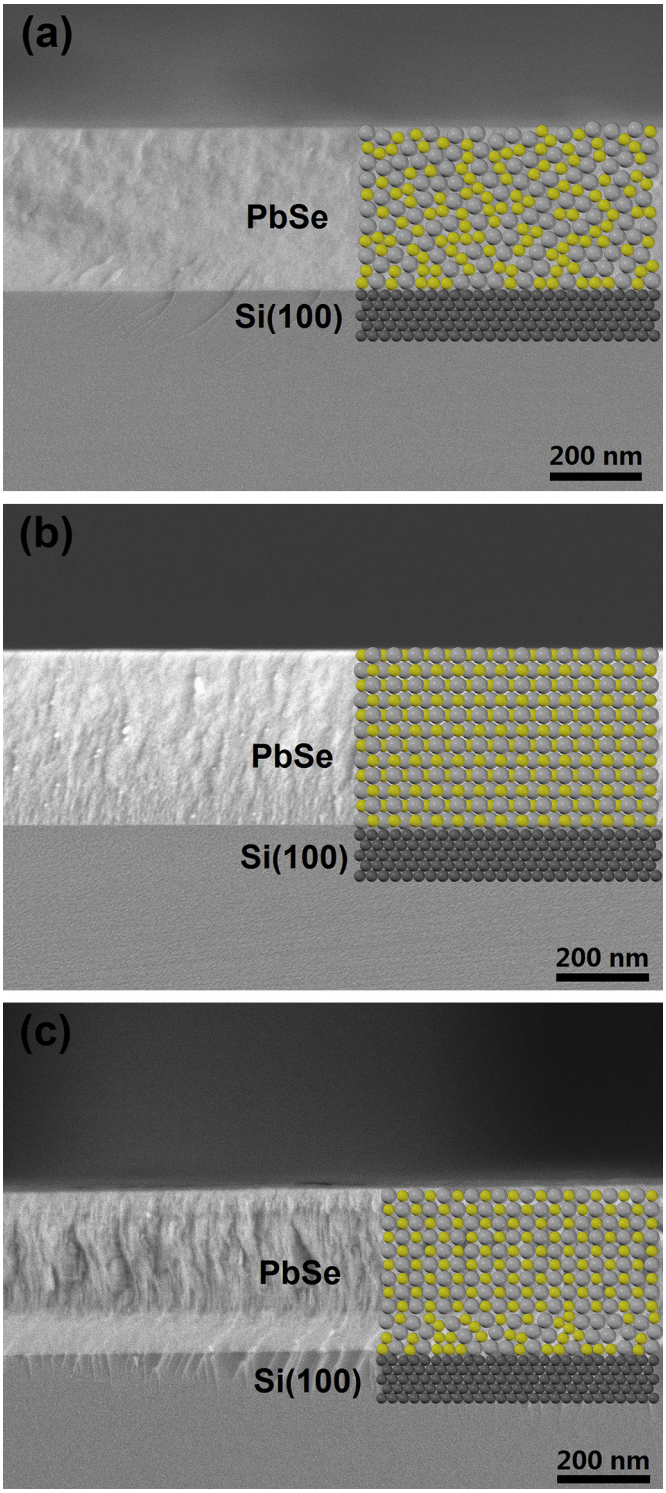


**Fig. 1.** Cross-section FE-SEM images of the sputtered PbSe thin films: (a) PbSe-50; (b) PbSe-150; (c) PbSe-250. The insets show the schematic diagram of the crystal structure of the corresponding sputtered PbSe thin films, the dark gray, light gray and yellow balls represent the Si, Pb and Se atoms, respectively. (For interpretation of the references to color in this figure legend, the reader is referred to the web version of the article.)

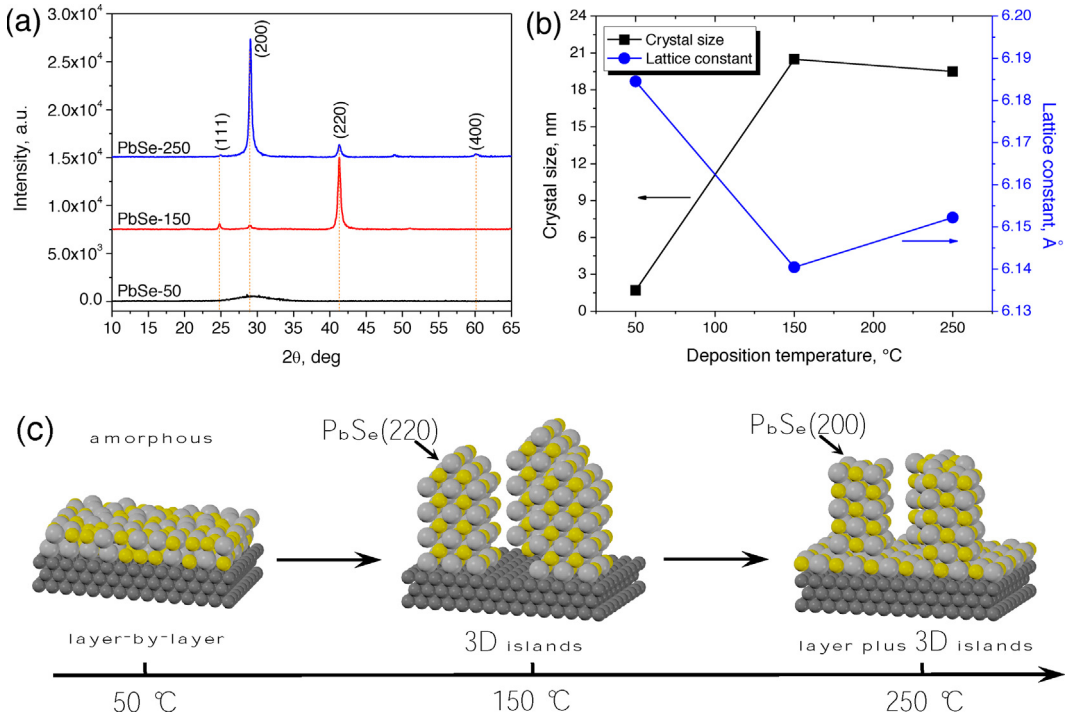


**Fig. 2.** (a) XRD results of the sputtered PbSe thin films prepared at different temperatures; (b) variation of the crystal size and lattice constant with the deposition temperature; (c) evolution of the growth mode and crystal structure with the deposition temperature. The dark gray, light gray and yellow balls represent the Si, Pb and Se atoms, respectively. (For interpretation of the references to color in this figure legend, the reader is referred to the web version of the article.)

3D islands formation due to the low diffusion activation energy of the Pb and Se atoms, as shown in Fig. 2(c).

The crystallinity of the sputtered PbSe thin films increases as the deposition temperature increases from 50 °C to 150 °C, and the main diffraction peak is attributed to PbSe (2 2 0), indicating that the main grown direction is along the [2 2 0] crystal orientation at 150 °C. Moreover, the sputtered PbSe thin film prepared at 150 °C are composed of columnar grains, which may be attributed to the transition from the Frank–van der Merwe growth mode to the Volmer–Weber (or 3D island) growth mode as the deposition temperature increases from 50 °C to 150 °C, as shown in Fig. 2(c).

When the deposition temperature reaches to 250 °C, the main diffraction peak changed to PbSe (2 0 0), indicating that the dominating growth direction is along the [2 0 0] crystal orientation. It's interesting to note that a unique double-layer structure, nano-crystalline layer and columnar grain layer, is obtained at this temperature, which may be attributed to the Stranski–Krastanow (or layer plus 3D island) growth mode dominates at higher temperature, as shown in Fig. 2(c). Generally, the growth mode is dominated by the adsorption between the Pb, Se atoms and the substrates in the initial stages, which consequently leads to the formation of the nano-crystalline layer. When the film thickness reaches to a certain value (about 86 nm), a crystal structure transition from the nano-crystalline to the columnar grain is obtained due to the preferable adsorption between the Pb and Se atoms, and not with the substrates.

The average crystal size, $D$, of the sputtered PbSe thin films was calculated by using the Debye–Scherrer equation [24]:

$$D = \frac{0.9\lambda}{\beta \cdot \cos\theta} \quad (1)$$

where $\lambda$ denotes the wavelength of the X-ray radiation (Cu $K\alpha$, $\lambda = 1.5406$ Å), $\beta$ and $\theta$ represent the full width at half maximum and the Bragg diffraction angles of the peaks. Although the calculation for amorphous thin film (PbSe-50) may not be accurate, the variation tendency is reliable. The average crystal size increases sharply as the temperature increases from 50 °C to 150 °C, and then decreases slightly when the temperature reaches to 250 °C, as shown in Fig. 2(b) and Table 1, which may be attributed to the recovery and recrystallization process in the sputtered PbSe thin films at relatively high temperature [25].

The lattice constant, $a$, for the sputtered PbSe thin films with the cubic structure was calculated as:

$$a = d\sqrt{h^2 + k^2 + l^2} \quad (2)$$

where $d$ represents the distance between the $(h\,k\,l)$ atomic lattice planes. The lattice constant of the sputtered PbSe thin films varies from 6.1845 Å to 6.1404 Å with the deposition temperature, as shown in Fig. 2(b) and Table 1. Interestingly enough, the variation of the lattice constant with the deposition temperature is contrary to the variation of the average crystal size, indicating the micro-stain in the sputtered thin films also varied oppositely with the average crystal size.

The average micro-strain, $\varepsilon$, developed in the sputtered PbSe films was calculated by using the relation [26]:

$$\varepsilon = \frac{\beta \cot\theta}{4} \quad (3)$$

As listed in Table 1, the $\varepsilon$ values of the sputtered PbSe thin films decrease sharply as the crystallinity increases with the deposition temperature, indicating a lower number of lattice imperfections at higher deposition temperature, which is attributed to the decrease of the grain boundaries because of an increase in the average crystallite size of the film with increasing temperature.

### 3.2. Chemical composition

The content of the sputtered PbSe thin films was studied by using the energy dispersive X-ray detector (EDX) attached to the FE-SEM. As listed in Table 1, the content slightly deviates from the stoichiometric ratio, and the atomic content of the Se element is

**Table 1**
Thickness, EDX, XRD and optical band gap results of the sputtered PbSe thin films prepared at different temperatures.

| Samples | Thickness, nm | XRD | | | EDX | | | $E_g$, eV |
|---|---|---|---|---|---|---|---|---|
| | | $D$, nm | $a$, Å | $\varepsilon$, $10^{-3}$ | Pb, at.% | Se, at.% | O, at.% | |
| PbSe-50 | 390 | 1.7 ± 0.1 | 6.1845 | 43.06 | 43.71 | 47.83 | 8.46 | 0.235 |
| PbSe-150 | 416 | 20.5 ± 0.3 | 6.1404 | 4.99 | 44.68 | 46.15 | 9.17 | 0.252 |
| PbSe-250 | 370 | 19.5 ± 0.4 | 6.1522 | 5.28 | 45.39 | 46.03 | 8.58 | 0.244(0.346) |

higher than the Pb element, which may be attributed to the easier sputtering of the Se atoms and consequently the higher concentration in the PbSe thin films [27]. Moreover, the stoichiometric deviation decreases as the deposition temperature increases due to the higher volatility of the Se atoms than the Pb atoms on the film surface, which leads to the partial loss of the Se element in the sputtered PbSe thin films [28], indicating the effectiveness of modifying the content of the sputtered PbSe thin films by changing the deposition temperature. The oxygen contained in the thin films is probably attributed to the oxide layer on the film surface when exposed to the air, which is confirmed by the following XPS results.

Generally, the optical properties of the sputtered PbSe thin films are intensively affected by the chemical states of the existing elements. Within this research, the deposition temperature is relatively high, which may lead to the oxidation of the thin films considering the low base vacuum degree of $5 \times 10^{-3}$ Pa. Besides, the surface of the thin films can be oxidized when exposed to the air, which may lead to the formation of n-type inversion layer and consequently resulting in an ohmic behavior of the metal/semiconductor contact [29]. Hence, further XPS measurements were performed on the surface of the sputtered PbSe thin films before and after the $Ar^+$ etching treatment, in order to determine the chemical states of the Pb and Se elements, as shown in Fig. 3.

According to the XPS spectra obtained before the etching treatment, both the Pb and Se elements have two chemical states, PbSe (at 142.24 eV and 137.37 eV), PbO (at 142.79 eV and 138.14 eV) and PbSe (at 53.95 eV and 53.11 eV), $SeO_2$ (at 58.67 eV), respectively, indicating the formation of the oxide layer on the film surface. After the etching treatment, the oxides of the Pb and Se elements disappear, just one chemical state, PbSe, exists in the sputtered PbSe thin films, which means no oxides were created during the deposition process.

### 3.3. Optical properties

As mentioned above, the PbSe thin films are mainly used as mid-infrared detector materials due to the intensive absorption in the infrared range. Within this research, the FT-IR absorption spectra of the sputtered PbSe thin films were recorded in the wavenumber range between 4000 $cm^{-1}$ (2.5 μm) and 400 $cm^{-1}$ (25 μm) at room temperature, as shown in Fig. 4(a).

The absorption edges of these three sputtered PbSe thin films are similar, located at about 2000 $cm^{-1}$ (5 μm) which is in agreement with the results in Ref [24]. However, it is interesting to note that the sputtered PbSe thin film prepared at 250 °C shows a unique absorption at about 3200 $cm^{-1}$ (about 3.1 μm), which is attributed to its double-layer structure, especially the absorption of the nano-structured layer next to the substrates.

The optical band gap, $E_g$, is an essential parameter to characterize the optical and photoelectric properties of the semiconductor materials, which can be calculated as follows [30]:

$$(\alpha h\nu)^{1/n} = B(h\nu - E_g) \quad (4)$$

where $\alpha$ is the absorption coefficient, which can be calculated as $\alpha = 1/d\ln(I_0/I)$, where $I_0$ denotes the incident beam intensity and $I$ is the beam intensity after traversing certain thickness, $d$, of the thin films; $h\nu$ represents the incident beam energy; $B$ is a constant; $n$ is an exponent, which can be 1/2, 3/2, 2 and 3 depending on the type of the electrons transition at the absorption edge: allowed direct transition $n = 1/2$, forbidden direct transition $n = 3/2$, allowed indirect transition $n = 2$ and forbidden indirect transition $n = 3$. The electrons in the PbSe materials obey the direct transition ($n = 1/2$) at the absorption edge, hence, the optical band gap of the sputtered PbSe thin films can be represented as follows:

$$(\alpha h\nu)^2 = B(h\nu - E_g) \quad (5)$$

As shown in Table 1, the $E_g$ values of the sputtered PbSe thin films change with the deposition temperature, which is attributed to the different crystal structures obtained at different deposition temperature. Moreover, the $E_g$ variation is contrary to the lattice constant, which is due to the present of the oxygen atoms on the thin films surface, confirmed by the simulation results shown in Section 3.4. It is interesting to note that the sputtered PbSe thin film prepared at 250 °C has two optical band gap values, 0.244 eV and

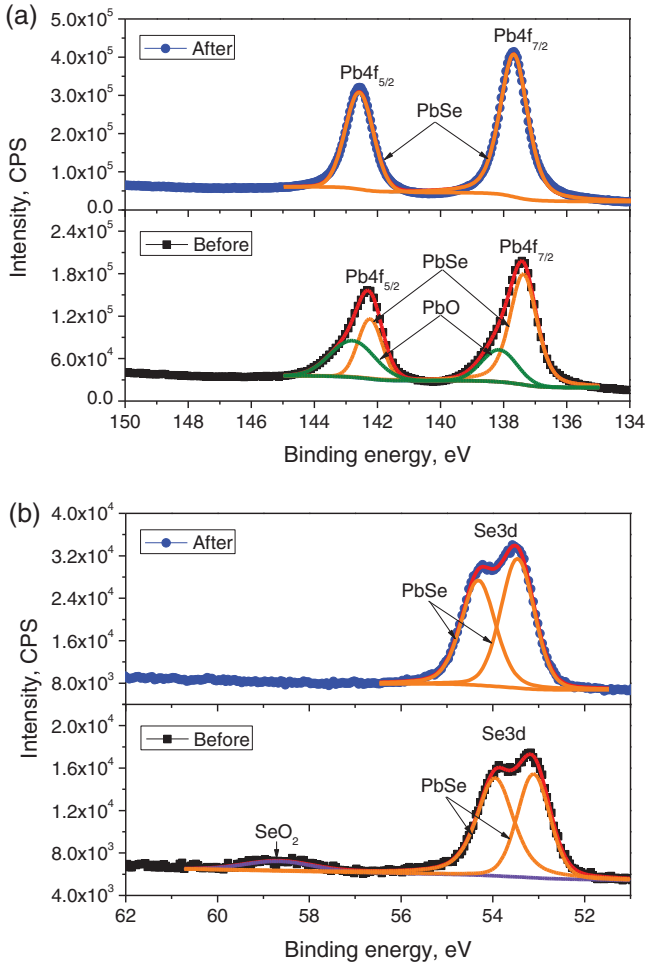


**Fig. 3.** XPS results of the sputtered PbSe thin films before and after the surface is etched by $Ar^+$: (a) Pb4f spectra; (b) Se3d spectra.

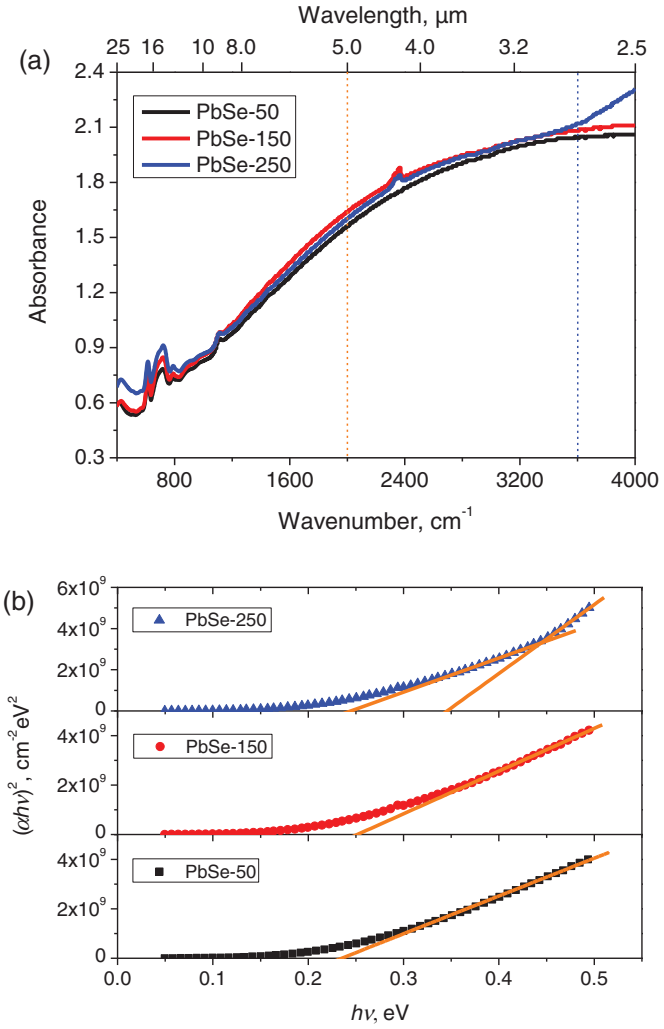


**Fig. 4.** Optical properties of the sputtered PbSe thin films prepared at different temperatures: (a) FT-IR absorption spectra; (b) calculation of the optical band gap.

0.346 eV, which are attributed to the different infrared absorption of the double-layer structure. The nano-crystalline layer near the substrate is responsible for the short wavelength absorption, i.e., the $E_g$ value of this PbSe layer is 0.346 eV, while the columnar-grain layer is related to the long wavelength absorption, i.e., the $E_g$ value of this PbSe layer is 0.244 eV [23].

### 3.4. Discussion

As mentioned above, the optical properties of the sputtered PbSe thin films are significantly affected by their microstructure, hence, it is essential to study the influences of the deposition temperature on the grown mechanism. Generally, the film growth is driven by the difference in total free energy per unit volume, $\Delta E$, which depends on the interface, surface, and strain contributions as follows [31]:

$$\Delta E = \Delta E_{\text{interface}} + \Delta E_{\text{surface}} + \Delta E_{\text{strain}} \quad (6)$$

where $\Delta E_{\text{interface}}$, $\Delta E_{\text{surface}}$, and $\Delta E_{\text{strain}}$ represent the interface, surface, and strain energy density differences between two neighboring grains, respectively. For the growth of the sputtered polycrystalline PbSe thin films, the interface energy contribution can be neglected. Hence, the growth mode is mainly dominated by the surface and strain energy contributions, and it is essential to determine which one is more significant under given conditions.

**Table 2**
Surface energy density of the PbSe (2 0 0) and (2 2 0) planes.

| Plane | $E_{\text{bulk}}$, eV | $E_{\text{slab}}$, eV | $A$, $10^{-20}$ m$^2$ | $E_{\text{surface}}$, J m$^{-2}$ |
|---|---|---|---|---|
| (2 0 0) | −1,920.84 | −1,7281.90 | 4.33 × 4.33 | 2.40 |
| (2 2 0) | −1,920.84 | −1,7271.50 | 6.12 × 4.33 | 4.84 |

Note: the lattice constant is the standard value for pure bulk PbSe materials.

For the polycrystalline thin films, the surface energy density, $\Delta E_{\text{surface}}$, and strain energy density, $\Delta E_{\text{strain}}$, contribution to the film growth can be represented as [31]:

$$\Delta E_{\text{surface}} = \frac{E_{hkl} - E_{h'k'l'}}{\delta} \quad (7)$$

$$\Delta E_{\text{strain}} = (M_{hkl} - M_{h'k'l'}) \cdot \varepsilon^2 \quad (8)$$

where $E_{hkl}$ and $E_{h'k'l'}$ denote the surface energy of two neighboring grains with <$h\,k\,l$> and <$h'\,k'\,l'$> orientation, respectively; $\delta$ is the thickness of the thin films; $M_{hkl}$ and $M_{h'k'l'}$ represent the elastic biaxial modulus of two neighboring grains with <$h\,k\,l$> and <$h'\,k'\,l'$> orientation; $\varepsilon$ is the micro-strain of the thin film.

Within this research, the surface energy of the PbSe (2 0 0) and (2 2 0) planes was calculated using the generalized gradient approximation (GGA) by Perdew–Burke–Ernzerhof (PBE). The (2 0 0) and (2 2 0) surfaces were simulated using a slab with nine layers thickness, which was separated from repeated replicas by a certain vacuum thickness of 20 Å, as shown in Fig. 5(a) and (b). In this method, the surface energy of the planes was represented as [32]:

$$E_{\text{surface}} = \frac{E_{\text{slab}} - N_{\text{slab}}/N_{\text{bulk}} E_{\text{bulk}}}{2A} \quad (9)$$

where $E_{\text{slab}}$ is the total energy of the simulated slab; $E_{\text{bulk}}$ denotes the total energy of the bulk which has the same atomic ratio as the slab; $N_{\text{slab}}$ and $N_{\text{bulk}}$ represent the atom numbers within the slab and bulk; $A$ indicates the surface area of the simulated slab, and the number 2 accounts for the two surfaces in the slab. The surface energy of the PbSe (2 0 0) and (2 2 0) plane is 2.4 J m$^{-2}$ and 4.84 J m$^{-2}$, respectively, as shown in Table 2, indicating that PbSe (2 0 0) is the main growth plane when the surface energy is the dominating factor.

In order to obtain the elastic constants of the PbSe material, a supercell containing 64 atoms was built, and also calculated using the PBE + GGA functional. Usually, the effective elastic modulus, $M_{hkl}$, for the polycrystalline thin films is calculated by two averaging schemes due to the deviation from the single crystals [33]:

$$M^V_{hkl} = c_{11} + c_{12} - c_0\Gamma_{hkl} - \frac{2(c_{12} + c_0\Gamma_{hkl})^2}{c_{11} - 2c_0\Gamma_{hkl}} \quad (10)$$

$$M^R_{hkl} = \frac{1}{s_{11} + s_{12} - s_0\Gamma_{hkl}} \quad (11)$$

where $M^V_{hkl}$ and $M^R_{hkl}$ denote the effective elastic modulus based on Voigt and Reuss averaging schemes, respectively; $c_{ij}$ ($i = 1, 4, j = 1, 2, 4$) and $s_{ij}$ ($i = 1, 4, j = 1, 2, 4$) represent the effective elastic stiffness and compliances of the thin films, respectively, as listed in Table 3 [34]; $c_0 = c_{11} - c_{12} - c_{44}$, $s_0 = s_{11} - s_{12} - s_{44}/2$; $\Gamma_{hkl}$ is the orientation factor for the [$h\,k\,l$] axis represented as:

$$\Gamma_{hkl} = \frac{h^2k^2 + k^2l^2 + l^2h^2}{\left(h^2 + k^2 + l^2\right)^2} \quad (12)$$

Generally, the average value of $M^V_{hkl}$ and $M^R_{hkl}$, also known as Voigt–Reuss–Hill average, $M^{VRH}_{hkl}$, is used to clarify the elastic properties of different orientations due to the inconsistent of $M^V_{hkl}$ and $M^R_{hkl}$ for certain planes, such as (2 2 0), (3 1 1), etc. [35]. Hence, the effective elastic modulus and the strain energy density of the PbSe (2 0 0) and (2 2 0) planes can be obtained using equations (8), (10)

**Table 3**
Elastic constants of the PbSe crystals.

| Sample | $c_{11}$, GPa | $c_{12}$, GPa | $c_{44}$, GPa | $s_{11}$, $10^{-3}$ 1/GPa | $s_{12}$, $10^{-3}$ 1/GPa | $s_{44}$, $10^{-3}$ 1/GPa |
|---|---|---|---|---|---|---|
| PbSe | 138.77 | 15.07 | 17.82 | 7.36 | −0.72 | 56.11 |

and (11), with the results are listed in Table 4. Obviously, the strain energy density of the (2 2 0) plane is much lower than the (2 0 0) plane at certain micro-strain, indicating that PbSe (2 2 0) is the main growth plane when the strain energy is the dominating factor.

Based on the above results, the contribution of the surface and strain energy density to the film growth at different deposition temperatures is shown in Fig. 6. It is interesting to note that the surface energy contribution is almost invariable with the deposition temperature, while the strain energy contribution decreases sharply as the deposition temperature increases. A critical point was obtained at about 180 °C, indicating that the strain energy contribution is more prominent when the deposition temperature is less than 180 °C, while, the surface energy contribution is more prominent when the deposition temperature is higher than 180 °C. Combined with the calculated surface and strain energy density results of the (2 0 0) and (2 2 0) planes, it was deduced that the dominating growth direction is along the [2 2 0] orientation when the deposition is less than 180 °C due to its lower strain energy density. On the contrary, the dominating growth direction is along the [2 0 0] orientation when the deposition temperature is higher than 180 °C due to its lower surface energy density, which is in agreement with the XRD results.

**Table 4**
Strain energy density of the PbSe (2 0 0) and (2 2 0) planes.

| Plane | $M^{V}_{hkl}$, GPa | $M^{R}_{hkl}$, GPa | $M^{VRH}_{hkl}$, GPa | $E_{strain}$, $10^{-3}$ GPa ($\varepsilon = 0.5\%$) |
|---|---|---|---|---|
| (2 0 0) | 150.57 | 150.57 | 150.57 | 3.76 |
| (2 2 0) | 102.80 | 85.95 | 94.38 | 2.36 |

Note: the micro-stain $\varepsilon = 0.5\%$ is an arbitrary reference value.

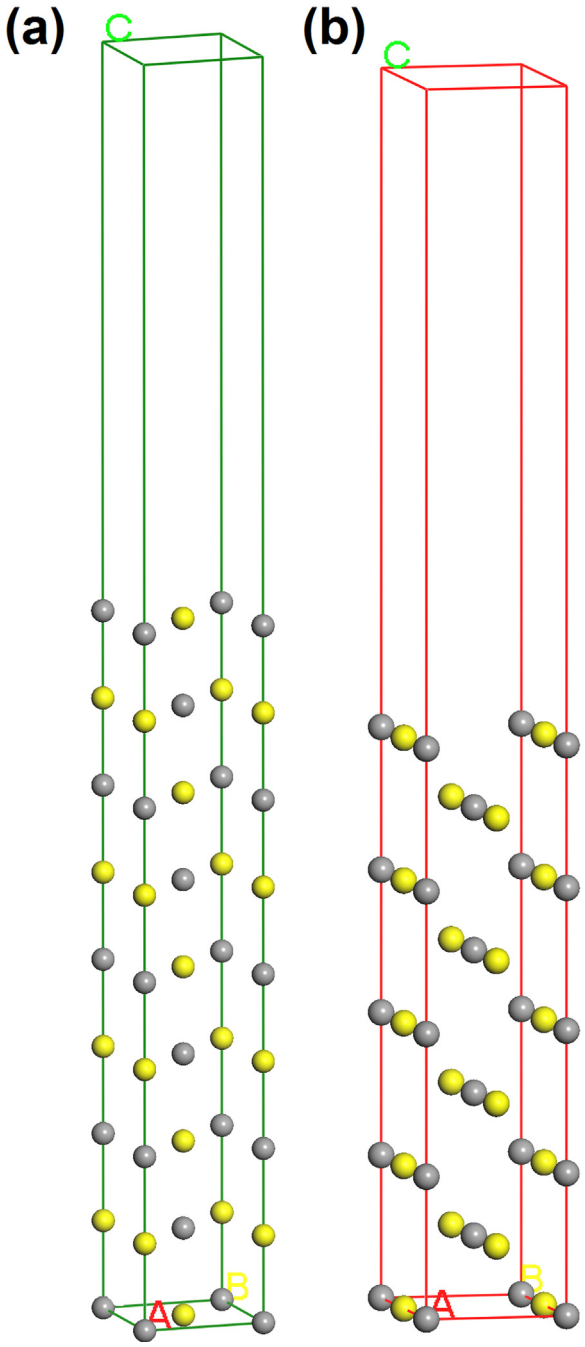


**Fig. 5.** Simulated structure of (a) (2 0 0) and (b) (2 2 0) surface slabs for the PbSe crystal. The light gray and yellow balls represent the Pb and Se atoms, respectively. (For interpretation of the references to color in this figure legend, the reader is referred to the web version of the article.)

As is known to all, the optical properties of the semiconductor materials are mainly determined by their band structure [24], especially the bands near the Fermi level. In this work, the band structure of the sputtered PbSe thin films was calculated using the first principles, and the effects of the microstructure on the band structure and density of states were studied in detail.

Three $Pb_{16}Se_{14}O_2$ supercells with the lattice constant of 6.1845 Å, 6.1404 Å and 6.1522 Å were built, respectively, and the oxygen atoms were added, based on the EDX and XPS results. The band structure and density of states (DOS) were calculated based on the generalized gradient approximation (GGA) with

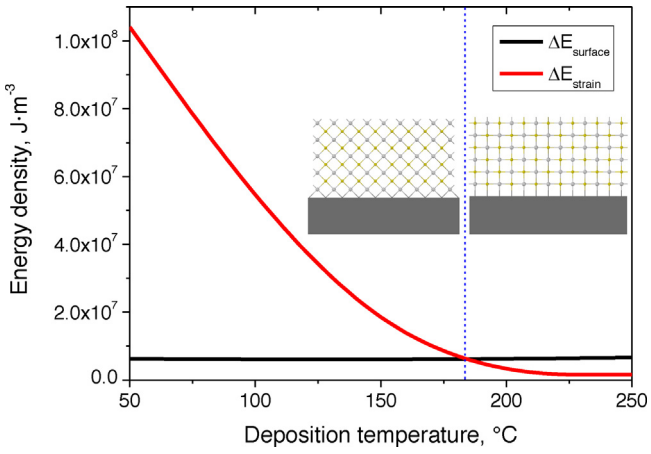


**Fig. 6.** Variation of the difference in surface energy density and in elastic strain energy density between two neighboring grains oriented along the [2 0 0] and [2 2 0] orientations as a function of the deposition temperature. The insets show the schematic diagram of the interface between PbSe and substrates with [2 2 0] and [2 0 0] growth orientations, and the light gray and yellow balls represent the Pb and Se atoms, respectively. (For interpretation of the references to color in this figure legend, the reader is referred to the web version of the article.)

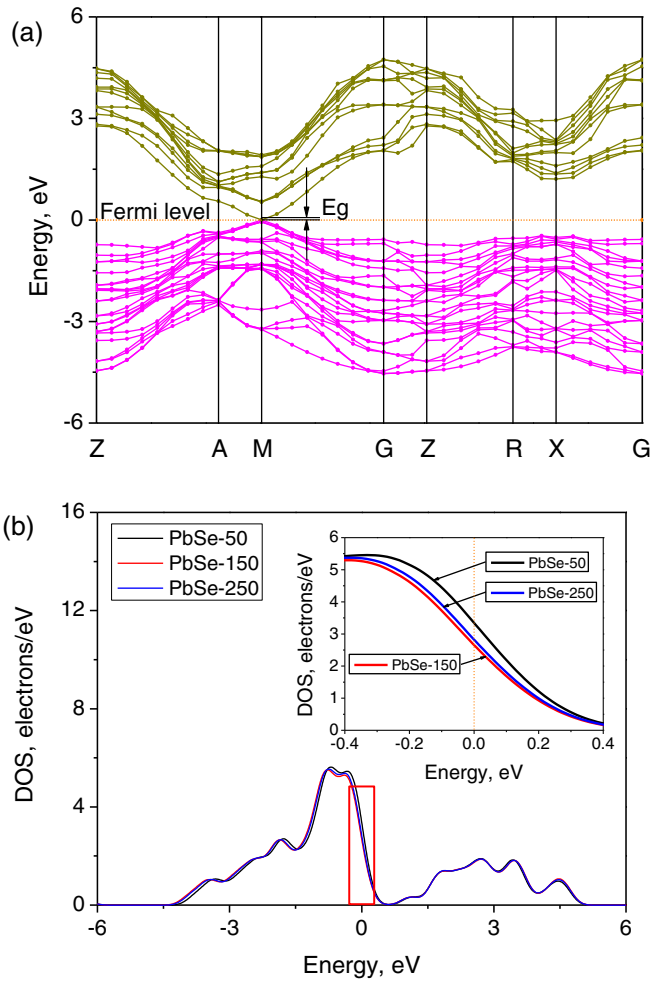


**Fig. 7.** (a) Band structure and (b) density of states (DOS) of the sputtered PbSe thin films. The inset shows the magnified view of the DOS near the Fermi level labeled by the rectangle.

Perdew–Burke–Ernzerhof (PBE) exchange correlation functional, as shown in Fig. 7.

The band structures of the PbSe thin films with different lattice are similar, and only PbSe-50 is shown in Fig. 7(a). The band gap of these three PbSe thin films varied from 0.005 eV to 0.079 eV and then to 0.072 eV as the lattice constant changed from 6.1845 Å to 6.1404 Å and then to 6.1522 Å, which is in agreement with the variation trend of the experimental values shown in Table 1. The underestimation of the calculated values is attributed to the generalized gradient approximation can not accurately describe the eigenvalues of the electronic states, however, the variation trend is reliable [36]. According to the DOS results shown in Fig. 7(b), the variation of the band gap is mainly determined by the shift of the valence band maximum near the Fermi level, while the conduction band minimum is almost unchanged with the lattice constant.

## 4. Conclusions

Three PbSe thin films were deposited on the Si (1 0 0) substrates using magnetron sputtering at 50 °C, 150 °C and 250 °C, respectively. The crystal structure of the sputtered PbSe thin films varies from the amorphous structure to the columnar grain structure, and then to the double-layer structure (nano-crystalline layer and columnar grain layer) as the deposition temperature increases from 50 °C to 250 °C due to the dominating growth mode changes from the Frank–van der Merwe (or layer-by-layer) growth mode to the Volmer–Weber (or 3D island) growth mode, and then to the Stranski–Krastanow (or 3D island-on-wetting-layer) growth mode. The growth mechanism of the sputtered PbSe thin films is mainly dominated by the surface and the strain energy contributions. Moreover, the strain energy contribution is more prominent when the deposition temperature is less than 180 °C, while, the surface energy contribution is more prominent when the deposition temperature is higher than 180 °C, which leads to the main growth direction along PbSe (2 2 0) at lower 180 °C and PbSe (2 0 0) at higher 180 °C due to the differences of the surface and the strain energy density between these two planes.

The absorption spectra of the sputtered PbSe thin films are in the 3.1–5 μm range, corresponding to the mid-infrared range. Moreover, the sputtered PbSe thin film prepared at 250 °C has two different optical band gaps due to its unique double-layer structure, which considerably expand the absorption range. According to the theoretical calculation results, the variation of the band gap with the deposition temperature is determined by the shift of the valence band maximum near the Fermi level with the lattice constant.

## Acknowledgments

This work was supported by the National Natural Science Foundation of China (51271022), the Fok Ying Tung Education Foundation (132001) and the Fundamental Research Funds for the Central Universities (FRF-TP-14-008A2). Alex Volinsky acknowledges support from the National Science Foundation under the IRES 1358088 grant.

## References

[1] E.A. Albanesi, E.L. Peltzer y Blanca, A.G. Petukhov, Calculated optical spectra of IV-VI semiconductors PbS, PbSe and PbTe, Comp. Mater. Sci. 32 (2005) 85–95.
[2] Q. Zeng, J. Shi, G. Jiang, M.L. Yang, F. Wang, J. Chen, Structures optical absorptions of PbSe clusters from ab initio calculations, J. Chem. Phys. 139 (2013) 094305–194305.
[3] M.F. Kotkata, M.S. Al-Kotb, I.G. El-Houssieny, Observation of the Meyer-Neldel rule in nanocrystalline PbSe thin films, Phys. Scr. 89 (2014) 115805.
[4] L. Zhang, Y. Zhang, S.V. Kershaw, Y.H. Zhao, Y. Wang, Y.H. Jiang, T.Q. Zhang, W.W. Yu, P.F. Gu, Y.D. Wang, H.Z. Zhang, A.L. Rogach, Colloidal PbSe quantum dot-solution-filled liquid-core optical fiber for 1.55 μm telecommunication wavelengths, Nanotechnology 25 (2014) 105704.
[5] T. Tohidi, K. Jamshidi-Ghaleh, Effect of TEA on photoluminescence properties of PbS nanocrystalline thin films, Appl. Phys. A 118 (2015) 1247–1258.
[6] J.J. Choi, Y.F. Lim, M.B. Santiago-Berrios, M. Oh, B.R. Hyun, L.F. Sun, A.C. Bartnik, A. Goedhart, G.G. Malliaras, H.D. Abruña, F.W. Wise, T. Hanrath, PbSe nanocrystal excitonic solar cells, Nano Lett. 9 (2009) 3749–3755.
[7] Z. Feit, J. Fuchs, D. Kostyk, W. Jalenak, Liquid phase epitaxy grown PbSnSeTe/PbSe double heterostructure diode lasers, Infrared Phys. Techn. 37 (1996) 439–443.
[8] V. Arivazhagan, M.M. Parvathi, S. Rajesh, Complementary NIR absorption of ZnSe induced by multiple PbSe submonolayers by vacuum deposition technique, Vacuum 99 (2014) 95–98.
[9] G. Springholz, T. Schwarzl, W. Heiss, T. Fromherz, G. Bauer, M. Aigle, H. Pascher, I. Vavra, Fabrication of 3.9-4.2 μm mid-infrared surface emitting PbSe/PbEuTe quantum dot lasers using molecular beam epitaxy, Physica E 13 (2002) 876–880.
[10] N. Mukherjee, A. Mondal, Comparative study on the properties of galvanically deposited nano- and microcrystalline thin films of PbSe, J. Electron. Mater. 39 (2010) 1177–1185.
[11] W.R. Feng, H. Zhou, F. Chen, Impact of thickness on crystal structure and optical properties for thermally evaporated PbSe thin films, Vacuum 114 (2015) 82–85.
[12] P.A. Loiko, G.E. Rachkovskaya, G.B. Zacharevich, V.S. Gurin, M.S. Gaponenko, K.V. Yumashev, Optical properties of novel PbS and PbSe quantum-dot-doped alumino-alkali-silicate glasses, J. Non-Cryst. Solids 358 (2012) 1840–1845.
[13] F. Zhao, S. Mukherjee, J. Ma, D. Li, S.L. Elizondo, Z. Shi, Influence of oxygen passivation on optical properties of PbSe thin films, Appl. Phys. Lett. 92 (2008) 1–3.
[14] P.J. McCann, I.N. Chao, H. Sachar, D. McAlister, C.P. Li, X.M. Fang, H.Z. Wu, K. Namjou, IV-VI semiconductor growth on silicon substrates and new mid-infrared laser fabrication methods, Spectrochim. Acta Part A 55 (1999) 1999–2005.
[15] Y.X. Yu, K.X. Zhang, Z. Li, S.Q. Sun, Synthesis and luminescence characteristics of DHLA-capped PbSe quantum dots with biocompatibility, Opt. Mater. 34 (2012) 793–798.

[16] W.L. Ma, J.M. Luther, H.M. Zheng, Y. Wu, A.P. Alivisatos, Photovoltaic devices employing ternary $PbS_xSe_{1-x}$ nanocrystals, Nano Lett. 9 (2009) 1699–1703.
[17] E.B. Salgado, M.T.S. Nair, P.K. Nair, R.A. Zingaro, Chemically deposited thin films of PbSe as an absorber component in solar cell structures, Thin Solid Films 519 (2011) 7432–7437.
[18] S. Gad, M.A. Rafea, Y. Badr, Optical and photoconductive properties of $Pb_{0.9}Sn_{0.1}Se$ nano-structured thin films deposited by thermal vacuum evaporation and pulsed laser deposition, J. Alloys Compd. 515 (2012) 101–107.
[19] R.T. Rumianowski, R.S. Dygdalab, W. Jungc, W. Bala, Growth of PbSe thin films on Si substrates by pulsed laser deposition method, J. Cryst. Growth 252 (2003) 230–235.
[20] H.Z. Wu, X.M. Fang, R. Salas Jr., D. McAlister, P.J. McCann, Transfer of PbSe/PbEuSe epilayers grown by MBE on $BaF_2$-coated Si(111), Thin Solid Films 352 (1999) 278–282.
[21] P.J. Kelly, R.D. Arnell, Magnetron sputtering: a review of recent developments and applications, Vacuum 56 (2000) 159–172.
[22] W.R. Feng, X.Y. Wang, H. Zhou, F. Chen, Effects of sputtering power on properties of PbSe nanocrystalline thin films deposited by RF magnetron sputtering, Vacuum 109 (2014) 108–111.
[23] M. Shandalov, J.P. Makai, J. Balazs, Z.s.J. Horvath, N. Gutman, A. Sa'ar, Y. Golan, Optical properties of size quantized PbSe films chemically deposited on GaAs, Eur. Phys. J. Appl. Phys. 41 (2007) 75–80.
[24] J.X. Si, J. Zhao, G.C. Dinga, H.F. Wu, Morphological evolution and growth mechanism of hierarchical structure of PbTe films grown by off-axis magnetron co-sputtering, Appl. Surf. Sci. 321 (2014) 233–239.
[25] L.P. Biró, A.L. Darabont, P. Fitori, The influence of thermal annealing on the physical properties of chemically deposited PbSe films, Europhys. Lett. 6 (1987) 691–696.
[26] A. Begum, A. Hussain, A. Rahman, Effect of deposition temperature on the structural and optical properties of chemically prepared nanocrystalline lead selenide thin films, Beilstein J. Nanotechnol. 3 (2012) 438–443.
[27] Y.I. Ravich, B.A. Efimova, I.A. Smirnov, Semiconductoring Lead Chalcogenides, Springer Science + Business Media, New York, 1970.
[28] E.I. Rogacheva, T.V. Tavrina, S.N. Grigorov, O.N. Nashchekina, V.V. Volobuev, A.G. Fedorov, K.A. Nasedkin, M.S. Dresselhaus, Effect of oxidation on the thermoelectric properties of PbSe thin films, J. Electron. Mater. 4 (2003) 298–303.
[29] O. Dos Santos, V. Mathet, C. Fau, S. Charar, M. Averous, Pb/p-PbSe junction: an investigation of current-voltage and capacitance-voltage measurements, Solid-State Electron 39 (1996) 813–819.
[30] A.A. Al-Ghamdi, S. Al-Heniti, S.A. Khan, Structural, optical and electrical characterization of Ag doped lead chalcogenide (PbSe) thin films, J. Lumin. 135 (2013) 295–300.
[31] V. Consonni, G. Rey, H. Roussel, D. Bellet, Thickness effects on the texture development of fluorine-doped SnO2 thin films: the role of surface and strain energy, J. Appl. Phys. 111 (2012) 033523–133523.
[32] L. Hammerschmidt, M. Quennet, K. Töpfer, B. Paulus, Low-index surfaces of $CoSb_3$ skutterudites from first principles, Surf. Sci. 637–638 (2015) 124–131.
[33] F. Huang, M.L. Weaver, Biaxial modulus of fiber-textured cubic polycrystalline films with an arbitrary texture axis [hkl], J. Appl. Phys. 98 (2005) 073505–173505.
[34] M. Lach-hab, D.A. Papaconstantopoulos, M.J. Mehl, Electronic structure calculations of lead chalcogenides PbS, PbSe, PbTe, J. Phys. Chem. Solids 63 (2002) 833–841.
[35] H.P. Wu, L.Z. Wu, J.F. Hui, X. Jin, S.Y. Du, Effective biaxial modulus and strain energy density of ideally (hkl)-fiber-textured cubic polycrystalline films, Appl. Surf. Sci. 254 (2008) 4067-4074.
[36] G. Naeemullah, R. Murtaza, N. Khenata, S. Hassan, M.N. Naeem, S. Khalid, Bin Omran Structural and optoelectronic properties of $PbS_xSe_{1-x}$ $PbS_xTe_{1-x}$ and $PbSe_xTe_{1-x}$ via first-principles calculations, Comp. Mater. Sci. 83 (2014) 496–503.